J. Fluid Mech., page 1 of 19 © Cambridge University Press 2009
doi:10.1017/S002211200999231X

Experimental study on the kinetics of granular gases under microgravity

SOICHI TATSUMI[1]†, YOSHIHIRO MURAYAMA,[2]
HISAO HAYAKAWA[3] AND MASAKI SANO[1]

[1]Department of Physics, The University of Tokyo, 7-3-1 Hongo, Bunkyo-ku, Tokyo 113-0033, Japan

[2]Department of Applied Physics, Tokyo University of Agriculture and Technology, 2-24-16 Naka-cho, Koganei-shi, Tokyo 184-8588, Japan

[3]Yukawa Institute for Theoretical Physics, Kyoto University, Sakyo-ku, Kyoto 606-8502, Japan

(Received 12 August 2008; revised 7 September 2009; accepted 20 September 2009)

The kinetics of granular gases, including both freely cooling and steadily driven systems, is studied experimentally in quasi-two-dimensional cells. Under microgravity conditions achieved inside an aircraft flying parabolic trajectories, the frictional force is reduced. In both the freely cooling and steadily driven systems, we confirm that the velocity distribution function has the form $\exp(-\alpha|v|^{\beta})$. The value of exponent β is close to 1.5 for the driven system in a highly excited case, which is consistent with theory derived under the assumption of the existence of the white-noise thermostat (van Noije & Ernst, *Gran. Mat.*, vol. 1, 1998, p. 5764). In the freely cooling system, the value of β evolves from 1.5 to 1 as the cooling proceeds, and the system's energy decays algebraically ($T_g = T_0(1 + t/\tau)^{-2}$), agreeing with Haff's law (Haff, *J. Fluid Mech.*, vol. 134, 1983, p. 401430).

granular gas, kinetic theory, steady state, cooling state, microgravity, experiments Q1

1. Introduction

In recent years, interest in the rheological properties of granular material assemblies is rapidly growing. Granular systems exhibit solid, liquid or gas-like behaviours, depending on the external condition (Jaeger, Nagel & Behringer 1996; Duran 2000; Goldhirsch 2003). The different behaviours are owing to the difference in the dominant physical process of energy dissipation. In the gas-like state, so-called granular gas, energy dissipation is governed by inelastic collisions between particles. Many interesting behaviours such as cluster formations promoted by the instability of homogeneous state (Goldhirsch & Zanneti 1993; Kudrolli, Wolpert & Gollub 1997), chaotic behaviour (Baxter & Olafsen 2007) and the anomalous scaling of the pressure (Géminard & Laroche 2004; Falcon *et al.* 2006) are found. For granular gases, the dynamics can be understood as collections of binary collisions between granules and can be studied using the methods of the kinetic theory of gases based on the Boltzmann–Enscog equation.

In the granular gas system, since the kinetic energy of the system is dissipated by inelastic collisions, a non-equilibrium steady state is sustained by a continuous energy injection; we call this state a 'steady state'. When the energy injection is stopped, the system is brought into a freely evolving state. The system evolves from the steady state towards the resting state, where we call this transient state a 'cooling state'. If the

† Email address for correspondence: sk_tatsumi@issp.u-tokyo.ac.jp

system is spatially uniform, one can expect the existence of the scaling properties of the system during the 'cooling state'. The typical feature of granular gases appears in the statistical properties of the system, especially in the velocity distribution function (VDF), $f(v,t)$. Unlike the ideal gas system, in which the VDF is Gaussian, several experiments for granular gas systems exhibit non-Gaussian VDFs (Losert *et al.* 1999; Olafsen & Urbach 1999; Rouyer & Menon 2000; Baxter & Olafsen 2003; Painter, Dutt & Behringer 2003; van Zon *et al.* 2004; van Zon & MacKintosh 2005; Reis, Ingale & Shattuck 2007; Maaß *et al.* 2008).

The granular gas systems are widely studied both experimentally (Olafsen & Urbach 1998; Blair & Kudrolli 2001; Aranson & Olafsen 2002) and numerically (Murayama & Sano 1998; Das & Puri 2003; Kawarada & Hayakawa 2004; Miller & Luding 2004; Moon, Swift & Swinney 2004; Herbst *et al.* 2005; Ahmad & Puri 2006, 2007; Brilliantov *et al.* 2007; Wang & Menon 2008). It is known that the inelastic Boltzmann–Enskog equation is semi-quantitatively accurate to describe such granular gas systems (Jenkins & Richman 1985; Santos *et al.* 1989; Goldshtein & Shapiro 1995; Esipov & Pöschel 1997; van Noije & Ernst 1998; van Noije, Ernst & Brito 1998; Aspelmeier, Huthmann & Zippelius 2001; Jenkins & Zhang 2002; Brilliantov & Pöschel 2004; Goldhirsch, Noskowicz & Bar-Lev 2005; Ernst, Trizac & Barrat 2006; Mischeler, Mouhot & Richard 2006; Mischeler & Mouhot 2006; Pöschel, Brilliantov & Formella 2006; Villani 2006). The high energy tail of the VDF for the granular gas is predicted to be $\exp(-\alpha|v|^{\beta})$, where $\beta \neq 2$. The value of the exponent β in the steady state with the white-noise thermostat is $\beta = 3/2$, implying that random noise is applied frequently between collisions. On the other hand, β is 1 in the cooling state or the steady state with Gaussian thermostat, which is reduced to the velocity rescaling thermostat for molecular dynamics simulation in the small amplitude limit (Santos 2003). The non-Gaussian VDF of $\beta = 3/2$ is also derived in the dense system by a phenomenological approach based on the experimental results (Fiscina & Cáceres 2007).

However, two problems still remain unanswered among these studies. One is the lack of the systematic experiments in the cooling state. Although the evolution of granular temperature, the spatial correlation, the cluster formation and the VDF in the cooling state is numerically investigated (McNamara & Young 1994, 1996; Nie, Ben-Naim & Chen 2002; Kawahara & Nakanishi 2004; Hayakawa & Kawarada 2005), most experiments are performed in the steady state, except for a few studies (Losert *et al.* 1999; Painter *et al.* 2003; Maaß *et al.* 2008). Losert *et al.* (1999) have observed the VDF of $\beta = 1$ in the cooling state, where the velocity data are averaged across the entire cooling process, even though the total energy has dramatically changed in the course of the process. Theories (Haff 1983; Brilliantov & Pöschel 2000) predict that the kinetic energy of the system, called granular temperature T_g, algebraically decays as the cooling proceeds:

$$T_g = \frac{T_0}{(1 + t/\tau)^{\gamma}}, \tag{1.1}$$

where T_0 is the initial granular temperature, t is the time after the cooling starts and τ is a characteristic decay time. From the theoretical point of view (Brilliantov & Pöschel 2004), $\gamma = 2$ for hard particles whose restitution coefficient is independent of the relative velocity, while $\gamma = 5/3$ for viscoelastic particles whose restitution coefficient depends on the relative velocity. Quite recently, the time evolution of T_g with $\gamma = 2$ has been observed in an experiment that uses a technique called the magnetic levitation (Maaß *et al.* 2008). A few tens of particles are trapped in a magnetic potential, and particles are quickly forced to make clusters at the bottom of the potential. Therefore,

the particles outside the cluster are regarded as gaseous particles, and then their velocities outside the cluster are used to test how the granular temperature decays in the cooling state. Although their results agree with the theoretical prediction, the effect of the external potential is unclear, and a large number of particles are required to guarantee sufficient statistics. Another problem of previous studies is that the statistical properties in the steady state depend on the magnitude of excitation. In the case of high acceleration, the VDF of $\beta = 3/2$ has been observed (Losert *et al.* 1999; Rouyer & Menon 2000), which is consistent with the theory with the white-noise thermostat (van Noije & Ernst 1998; Santos 2003). On the other hand, in the case of low acceleration, such relations remain obscure. Although several papers indicated possible origins of the deviation such as the friction of the wall (van Zon *et al.* 2004) or the way in which the system is excited (van Zon & MacKintosh 2005), we still do not understand the matter at hand.

To check the validity of theoretical prediction and to obtain clear statistics on granular gases, inelastic collisions between particles should be dominant, where additional effects such as frictional forces or an external potential should be reduced. To this end, a part of our experiments is conducted under the microgravity condition. Under the normal gravity condition, for particles with small velocities, the dominant dissipation is not caused by the inelastic collisions but by the friction between particles and the wall of a container, since the collision rate is low. The microgravity condition suppresses the effect of friction against the wall, because the frictional force is proportional to the normal force. Falcon *et al.* (2006) have studied a three-dimensional granular gas under microgravity condition and succeeded in obtaining the probability distribution function of the collision frequency between the particle and the wall.

Under the normal gravity condition, we have used quasi-two-dimensional cells with a rough top plate for the excitation of particles and a smooth bottom plate to facilitate rolling motions of particles after the vertical vibration has stopped. Because the rolling friction is much smaller than the sliding one, we can reduce frictional force.

The microgravity condition allows us to create an ideal state for granular gases, in particular for the cooling state. There is good agreement between the theory and our experiments in both the energy decay and the shape of the VDF under the microgravity condition, whereas the agreement is not clear under the normal gravity condition.

The organization of this paper is as follows. The experimental setup and analytic methods in our experiments are, respectively, explained in §§2 and 3. The experimental results for the steady state and the cooling state are shown in §§4 and 5, respectively. Finally, we discuss and conclude our report in §6. In Appendix A, we estimate the role of the hydrodynamic interaction among particles. In Appendix B, we evaluate the degree of g-jitter during the experiments under the microgravity condition.

2. Experimental setup

2.1. *Materials*

The experimental setups are presented in figure 1. Mono-dispersed zirconium beads (ZnO_2, diameter $d = 1.00\,\mathrm{mm} \pm 0.05\,\mathrm{mm}$; Toray Industries, Inc.) are confined in quasi-two-dimensional cells. The material constants of zirconium beads are shown in table 1. The restitution coefficient of a bead with a glass plate, ε_{gl}, and that with a zirconium plate, ε_{zir}, are determined by measuring the speeds before and after a collision with the plate. The restitution coefficient determined by a particle–plate collision is usually

	ρ (g cm^{-3})	E (MPa)	Y (MPa)	ε_{gl}	ε_{zir}	Γ_{zir} (mJ m^{-2})
ZrO_2	6.0	210	780	0.981 (2)	0.954 (27)	41∼45

TABLE 1. Material constants of working granules, Zirconium beads. ρ, E, Y, ε_{gl}, ε_{zir}, and Γ_{zir} are density, Young's modulus, yield stress, restitution coefficient between glass plate and zirconium bead, restitution coefficient between zirconium plate and zirconium bead, and surface energy of zirconium, respectively. ρ, E, and Y are obtained from the datasheet or the information from Toray Industries, Inc. We refer to the experimental study by Król & Król (2006) for the value of Γ_{zir}.

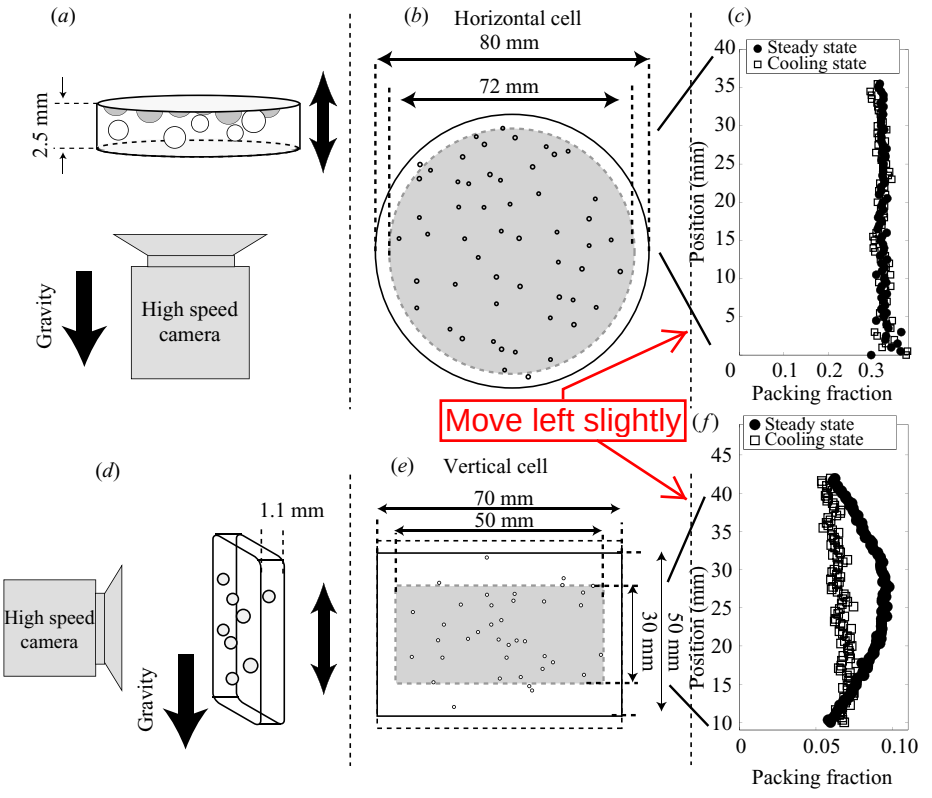

FIGURE 1. Setups for (*a–c*) the horizontal cell and (*d–f*) the vertical cell. (*a*, *d*) Schematic diagram of the cells. (*b*, *e*) Top views of the cells. The grey zones in (*b*, *e*) are used for our analysis, namely the region of interest. (*c*, *f*) The time-averaged area fractions of particles are plotted as a function of the distance from the centre for the horizontal cell and as a function of the position along the vertical axis for the vertical cell.

larger than that determined by a particle–particle collision. For aluminium and brass materials, Weir & Tallon (2005) report that restitution coefficient of the particle–particle collision is about 80 % of that of the particle–plate collision. Hence, we regard the restitution coefficient between zirconium beads as $0.8\,\varepsilon_{zir}$. A tangential frictional coefficient μ between particles is usually less than 0.2; Labous, Rosato & Dave (1997) showed a typical value of μ being 0.175. Therefore, we can use the theory of Jenkins & Zhang (2002), in which the frictional effect can be absorbed by the suppression of the effective restitution coefficient $\varepsilon_{eff} = \varepsilon - \frac{\pi}{2}\mu + \frac{9}{2}\mu^2$. The quantitative validity of this theory has been extensively studied by Saitoh & Hayakawa (2007).

Thus, we can estimate that ε_{eff} for a binary collision of zirconium beads is 0.62, assuming $\varepsilon = 0.8\,\varepsilon_{zir}$ and $\mu = 0.175$. In addition, the lower limit of the impact speed of a particle to stick to the plate is $1.25\,\mathrm{mm\,sec^{-1}}$ estimated from a value of Γ_{zir} (Thornton & Ning 1998), which is sufficiently small for our experimental conditions.

Thus, (i) the frictional effects can be absorbed in the effective restitution coefficient, and (ii) sticking force between the particle and the wall is negligible.

2.2. *Horizontal cell*

We use two types of quasi-two-dimensional cells: a horizontal cell and a vertical cell. The horizontal cell (figure 1*a*) is set in a horizontal plane and is accelerated vertically. The vertical cell (figure 1*b*) is set in a vertical plane and is accelerated vertically. The horizontal cell is a cylinder with a diameter of $80\,d$ and a depth of $2.5\,d$. The top plate and the sidewalls are made of aluminium, and the bottom plate consists of a glass plate coated with electrically conductive indium tin oxide (ITO) film to prevent static electrical charge. To randomize the motion of the particles, 1 mm diameter glass beads are glued to the top plate. The minimum gap between two plates is roughly $1.5\,d$, and the average gap is $1.8\,d$. The horizontal cell is used under both the microgravity and the normal gravity conditions. For the microgravity experiment, the number of particles confined in the cell is 2000 ± 5, the corresponding area fraction is 0.313 ± 0.001 (the error corresponds to an error bar in the weight per each particle due to small dispersion). For the normal gravity experiment, most of the experiments use the same number of particles, 2000 ± 5, except for several data sets with 1000 ± 3 and 3200 ± 10 particles which are performed to test the effect of area fraction. The cell is kept in vacuum condition (200–300 Pa at maximum) to avoid hydrodynamic interaction between particles. Under this condition, we estimate that the velocity reduction due to hydrodynamic drag between two collision events is roughly $6.6 \times 10^{-2}\,\mathrm{mm\,sec^{-1}}$ (see Appendix A). In both the steady state and the cooling state, the root mean square (rms) velocity of particles is sufficiently higher than this value. Therefore, the hydrodynamic effect is negligible in our setup.

External force is applied by sinusoidal acceleration using an electromagnetic vibration system (9514-AB/SD vibrator, EMIC Corp.). By the vertical vibration of the cell, all the particles gain high vertical velocity. When the particles strike the top plate, they are scattered and randomized by the glued beads. Because of the vertical vibration, the magnitude of the velocity of particles in the vertical direction is much larger than that in the horizontal direction. In our experiments, the horizontal components of the velocity are measured.

Under the normal gravity condition, the steady state is realized by setting the frequency f ranging from 70 to 200 Hz and the acceleration $A\omega^2$ ranging from to 10 to $200\,\mathrm{m\,sec^{-2}}$, where A is an amplitude of the vibration and $\omega = 2\pi f$ is an angular frequency. Under the microgravity, the frequency is fixed at 100 Hz, and the acceleration is varied from 6.0 to $48\,\mathrm{m\,sec^{-2}}$. Throughout the experiments, the acceleration is measured by a vibration accelerometer (VM-83, RION).

Moreover, to test the effect of the area fraction on the statistics of the system, the experiments on two other area fractions, 0.156 ± 0.001 ($N = 1000 \pm 3$) and 0.50 ± 0.01 ($N = 3200 \pm 10$), are conducted.

The cooling state is realized by the following procedure. First, we set the frequency to 100 Hz and the acceleration to $48\,\mathrm{m\,sec^{-2}}$ for more than 10 sec, then suddenly turn off the vibration. In the cooling experiments under the normal gravity, the particles roll on the bottom glass plate soon after the vertical vibration is stopped, indicating that the frictional effect is sufficiently reduced even under the normal gravity.

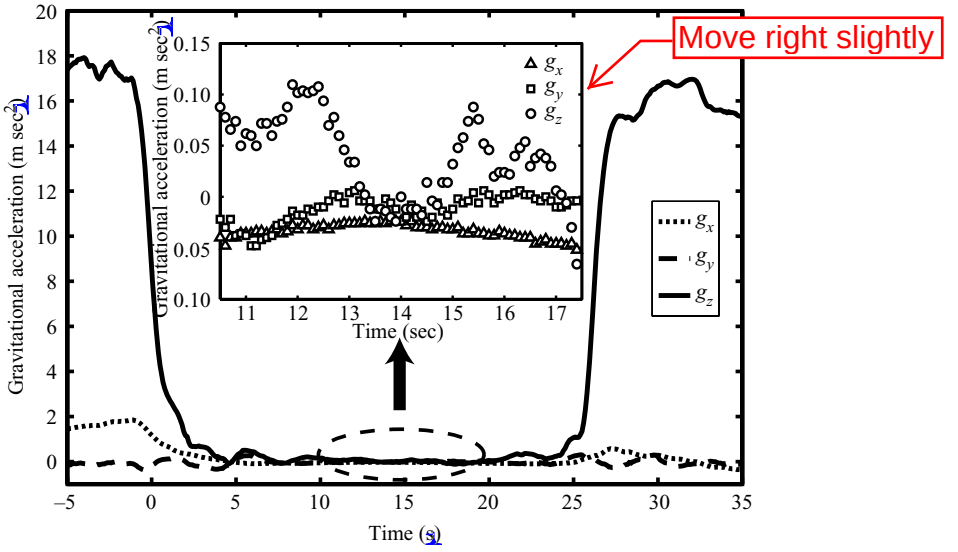

FIGURE 2. Time sequences of acceleration during a parabolic flight. The level of microgravity condition is maintained below 0.1 m sec^{-2}. The typical duration of the microgravity condition is about 20 sec. The experiments are conducted within about 10 sec of each microgravity period. The measurement time is 1.6 sec. Measurements are performed as the level of microgravity became lower and more stable. In total, about 100 data sequences are taken.

2.3. *Vertical cell*

As shown in figure 1(*b*), the vertical cell is a thin rectangular parallel-piped cell with an area of $50\,d \times 70\,d$ and a thickness of $1.1\,d$. The entire cell wall is made of glass plate coated with ITO film. The vertical cell is only used under the microgravity condition. The number of particles confined in the cell is fixed at 300, in which the corresponding area fraction is 0.067. This setup is similar to that in the experiment by Rouyer & Menon (2000) except for our use of the microgravity condition. The hydrodynamic effect is estimated in the same manner for the horizontal cell. Since the vertical cell is not in vacuum, its hydrodynamic effect is much larger than that of the horizontal cell. The velocity decrease between consecutive collisions is estimated as 4.2×10^{-1} mm sec^{-1}, which is sufficiently low compared with the rms velocity of particles. Thus, the hydrodynamic effect is also negligible in the vertical cell. Similar to the horizontal cell, the external force is applied by sinusoidal acceleration. Owing to the vertical acceleration, all the particles near the top and bottom boundaries gain high velocity towards the vertical direction. Then, particles reach the centre region after 2–3 collisions. Because of the sufficiently high acceleration and the microgravity condition, the density profile of the system becomes symmetric (see figure 1*b*). It is worth noting that the system becomes uniform in the cooling state. The steady state and the initial condition for the cooling state are realized with a fixed frequency of 40 Hz and a fixed acceleration of 250 m sec^{-2}.

2.4. *Microgravity condition*

A microgravity condition is achieved aboard a parabolic flight of a Gulfstream II jet aircraft (Diamond Air Service Co. and Japan Space Forum). Figure 2 shows an example of the microgravity process.

The fluctuation of microgravity is called g-jitter. The g-jitter in the z-direction, δg_z, is kept below about $0.1\,\mathrm{m\,sec^{-2}}$ for approximately 20 sec, and the xy directions, δg_x and δg_y, are kept under $0.03\,\mathrm{m\,sec^{-2}}$. However, δg_z does not affect our measurements because we analyse the motion of particles in the xy plane for the horizontal cell and that in the y-direction for the vertical cell. In the cooling experiments, we further choose a suitable condition in which the microgravity level becomes very low during the flights, and choose the appropriate data that include no average drift. Thus, we estimate that δg is $0.01\,\mathrm{m\,sec^{-2}}$ in the cooling experiments. This is validated by monitoring the mean velocity of particles in the cooling state; see Appendix B.

To estimate the effect of g-jitter, we introduce a ratio R:

$$R = \tau^* \frac{\delta g}{v_{th}}, \tag{2.1}$$

where τ^* is a characteristic time for the particle–particle or the particle–plate collisions, and v_{th} is the thermal velocity of particles, $v_{th} = \sqrt{\langle v_x^2 \rangle + \langle v_y^2 \rangle}$, where v_x and v_y are velocity components and $\langle \cdot \rangle$ denotes the average over all the particles. The estimation of R is discussed in the last part of §§4 and 5.

3. Analysis

3.1. *Particle tracking*

Particle motion is captured by a high-speed camera (1024PCI, PHOTRON), at a frame rate of 1 kHz. The size of the image is 1024×1024 pixels, and the spatial resolution is about $80\,\mu\mathrm{m\,pixel^{-1}}$ on the image. The particle size on the image is about 12 pixels, and the centroid of each particle is obtained with a precision of $0.007\,d$ ($7\,\mu$m). A simple algorithm for particle tracking is performed by detecting the nearest particle within a distance d between consecutive images. Thus, the particles with velocities less than $1\,\mathrm{m\,sec^{-1}}$ can be tracked. We calculate the velocity of each particle from the displacement in eight frames. This interval and the precision of the centroid determine the lower limit, $1\,\mathrm{mm\,sec^{-1}}$, in detecting velocity. For the horizontal cell, this simple algorithm enables us to detect more than 99.8 % of the particles. For the vertical cell, to detect particles with a high velocity, we firstly perform the simple tracking and remove detected trajectories. Secondly, we perform a more elaborated tracking algorithm by minimizing the sum of the displacements for the remaining particles. For particles with velocities less than $1\,\mathrm{mm\,sec^{-1}}$, the velocities are recalculated after obtaining their trajectories. Because of the absence of obstacles and a low area fraction in the vertical cell, collision events can be easily detected; thus, the velocities are obtained from the linear trajectories between collision events. Finally, we detect particles within the speed range, $0.2\,\mathrm{mm\,sec^{-1}} < v < 3\,\mathrm{m\,sec^{-1}}$. Typical trajectories in the horizontal cell under the microgravity are shown in figure 3.

From the data on the position and velocity of all particles, we can calculate the diffusion constant, the granular temperature and VDF. Based on the measurements error analysis by Xu, Reeves & Louge (2004), we estimate that the obtained granular temperature could be 27 % lower than the actual one in the horizontal cell, which is due to the scattering of particles by the obstacles within eight frames. However, in the vertical cell, since most collisions are detected, there is no underestimation of the velocity and the granular temperature.

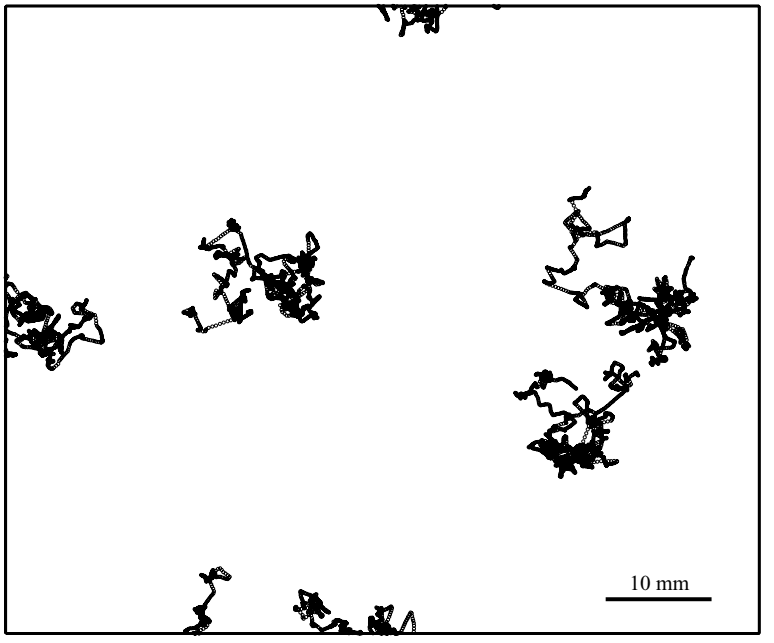

FIGURE 3. Typical trajectories of particles in the horizontal cell under the microgravity (steady state). Seven particles during 1.6 sec are picked up and shown. The frequency and the acceleration of external vibration are 100 Hz and $48\,\mathrm{m\,sec^{-2}}$, respectively.

3.2. *Calculation of velocity distribution function*

For the steady state, the velocity data for all particles across the measurement time of 1.6 sec are used for the calculation of the VDF. We then scale the velocity data by the rms velocity σ; we call the normalized velocity $c \equiv v/\sigma$. For the cooling state, σ decreases with time. We therefore calculate $\sigma(t)$ for every frame and obtain the VDF by averaging over every 50 msec.

Most VDFs satisfy the form, $f(c) = C\exp(-\alpha|c|^{\beta})$, where C is the normalization constant. From the normalization condition, $\int f(c)\,\mathrm{d}c = 1$ and $\int c^2 f(c)\,\mathrm{d}c = 1$, we can write the shape of VDF as

$$f(c) = \frac{\beta}{2}\frac{\Gamma(3/\beta)^{1/2}}{\Gamma(1/\beta)^{3/2}}\exp\left(-\left[\frac{\Gamma(3/\beta)}{\Gamma(1/\beta)}\right]^{\beta/2} c^{\beta}\right), \tag{3.1}$$

and consequently, only β is a fitting parameter. From the fitting of VDF by (3.1), we obtain the value of β for each VDF.

4. Steady state

4.1. *Granular temperature and diffusion constant*

The temperature and the diffusion constant are important physical quantities for the kinetic theory of molecular gas. In a weakly non-equilibrium time-dependent process, relaxation or dissipation is characterized by transport coefficients, e.g., diffusivity, viscosity and thermal conductivity. In the kinetic theory of collisional gases, all three of these transport coefficients are proportional to $v_{th}l$, where v_{th} is the thermal velocity and l is the mean free path. In this section, we focus on the granular temperature (T_g)

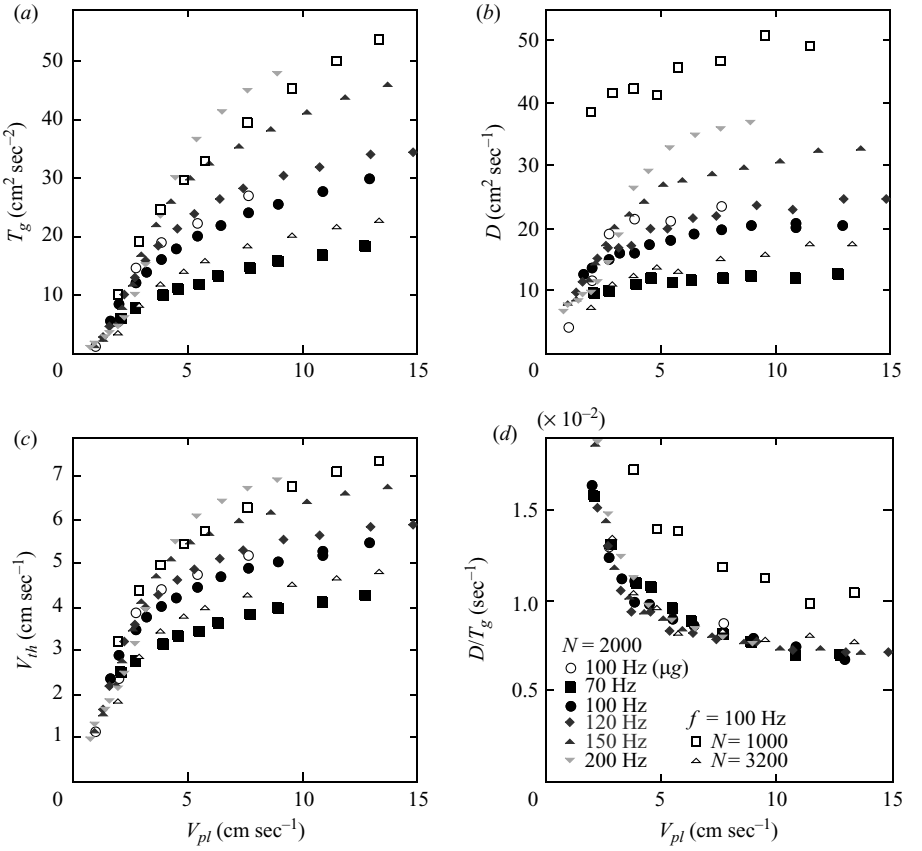

FIGURE 4. Dependence of (*a*) T_g, (*b*) D, (*c*) v_{th} and (*d*) D/T_g on v_{pl}, respectively. The legends in figure 4(*d*) are common to all figures.

and the diffusion constant (D) of particles in the steady state by an analogy between the granular system and the molecular gas. The granular temperature is defined as $T_g = \frac{1}{2}v_{th}^2$, where we subtracted the centre of mass velocity of all particles, $\bar{v}$, for the calculation of v_{th} to avoid mean drift effect. In our analysis, we set m as unity for simplicity. The diffusion constant is defined by, $D = \frac{d}{dt}\langle(\mathbf{x}(t) - \mathbf{x}(0))^2\rangle$, where $\mathbf{x}(t)$ is the position of a tracer particle at time t.

Figure 4 shows the dependence of various physical quantities on the maximum plate speed v_{pl} for the horizontal cell experiments. As shown in figures 4(*a*) and 4(*c*), the values of v_{th} are almost independent of the external frequency for small v_{pl}, while the values of v_{th} strongly depend on the external frequency for large values of v_{pl}. Moreover, the slope of v_{th} decreases as v_{pl} increases. Even if we plot T_g as a function of $A\omega^2$, the curves of T_g strongly depend on the frequency (data not shown). As shown in figure 4(*b*), D shows a monotonic increase with increasing v_{pl}. However, the dependencies of D on v_{pl}, $A\omega^2$ and T_g are not simple.

On the other hand, the value of D/T_g shows a good scaling relation on v_{pl} except for the lowest density case, $N = 1000$. This indicates that v_{pl} is a good parameter to characterize the nature of the system at a high enough density. Moreover, D/T_g seems constant in the case of excitation at a high degree (v_{pl} is large). It means that if the particles experience random forcing from the plate continuously, they

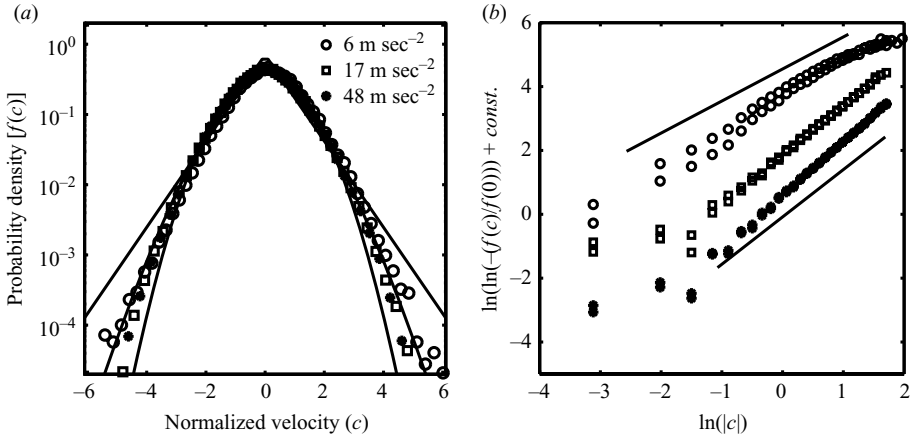

FIGURE 5. VDF obtained in the horizontal cell under the microgravity condition: $f = 100$ Hz. (a) The semi-log plot. (b) The double-logarithmic plot for the same result. The three lines in (a) represent reference data of the VDF with $\beta = 1$, 1.5 and 2. The two solid lines in (b) serve as a guide to the eyes for the slopes of 1.5 and 1. $f(0)$ is chosen as the experimental value for $c = 0$. The legends are common to all figures.

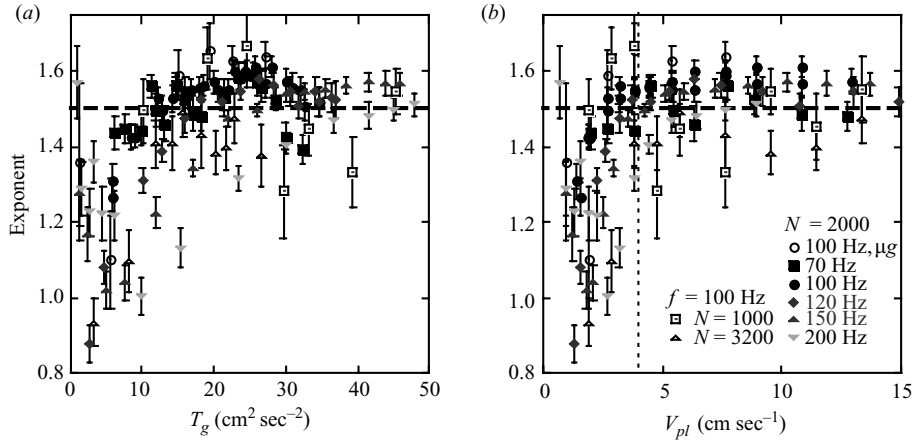

FIGURE 6. Dependence of the exponent β for the VDF on T_g (a) and v_{pl} (b). Dotted lines are to guide the eyes, and their value is 1.5. The legends are common for plots in both (a) and (b).

behave like Brownian particles. In such a case, the diffusivity of the particle should be proportional to its kinetic energy, i.e., D/T_g becomes a constant.

4.2. *Velocity distribution function*

Figures 5(a) and 5(b) show the VDFs under the microgravity condition in the horizontal cell. All VDFs show the form as in (3.1) for most of the velocity regions, where the exponent β depends on the external acceleration. The value of β increases from 1 to 1.5 with the increase of the external acceleration. This trend is clearly observed in figure 6(a) for both microgravity and normal gravity conditions, and among different densities.

These results are consistent with experimental studies on granular gases by Losert *et al.* (1999). In figure 6(b), the same data in figure 6(a) are plotted for v_{pl}. We note that the data collapse to $\beta = 1.55 \pm 0.05$ for high excitation cases ($v_{pl} > 4\,\mathrm{cm\,sec^{-1}}$),

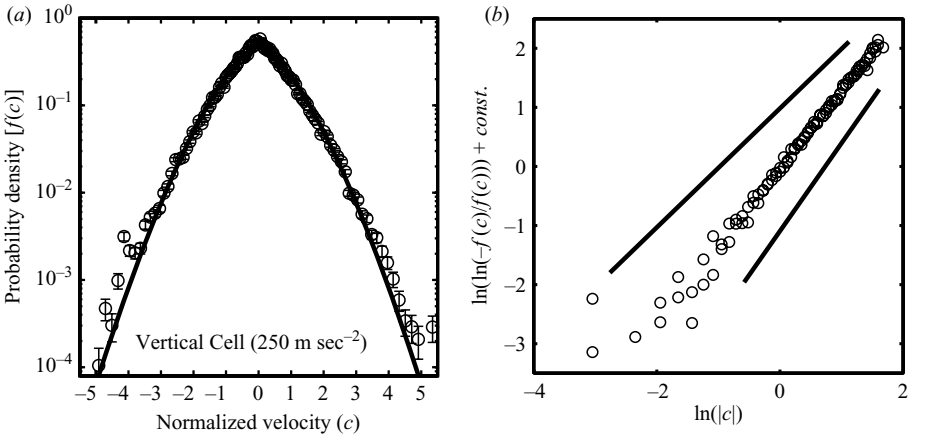

FIGURE 7. VDF obtained in the vertical cell under microgravity condition (open circles). $f = 40\,\mathrm{Hz}$ and $A\omega^2 = 250\,\mathrm{m\,sec^{-2}}$. (*a*) The semi-log plot. (*b*) The double-logarithmic plot for the same result. The solid line in (*a*) represents reference data of the VDF with $\beta = 1.5$. The two solid lines in (*b*) serve as a guide to the eyes for the slopes of 1.5 and 1. $f(0)$ is chosen as the experimental value for $c = 0$.

while the data are distributed in the range from 0.9 to 1.6 for low excitation cases ($v_{pl} < 4\,\mathrm{cm\,sec^{-1}}$). For high excitation cases, our results agree with the theory of van Noije & Ernst (1998), in which the VDF with $\beta = 1.5$ is derived for homogeneous and dilute granular gas excited by the white-noise thermostat.

4.3. *Results of the vertical cell*

In the vertical cell, the VDF for the steady state is obtained at $f = 40\,\mathrm{Hz}$ and $A\omega^2 = 250\,\mathrm{m\,sec^{-2}}$ under microgravity condition (figure 7). The VDF shows the form in (3.1), where the exponent $\beta = 1.28 \pm 0.04$ is obtained by fitting. The deviation from $\beta = 1.5$ can be caused by low excitation compared with the mean collision time.

4.4. *The effect of g-jitter*

In the steady state under the microgravity condition, the effect of g-jitter is estimated by R (see (2.1)) with $\delta g = 0.1\,\mathrm{m\,sec^{-2}}$. Under high enough excitation, τ^* is characterized by the mean collision time between a particle and the plate, defined as h/v_{pl}, where h is the distance between the top and bottom plates of the horizontal cell, and we obtain $R \simeq 10^{-2}$ for the acceleration, $f = 100\,\mathrm{Hz}$ and $A\omega^2 = 48\,\mathrm{m\,sec^{-2}}$. On the other hand, under low excitation, τ^* is characterized by the mean collision time between particles, defined as l/v_{th}, where l is the mean free path of a particle, and we obtain $R \simeq 10^{-1}$. Thus, we conclude that the effect of g-jitter is negligible in the steady state.

5. Cooling state

5.1. *Energy decay*

The cooling processes are observed about 1 sec after the external vibration is stopped. The initial conditions for the cooling processes are steady states (see § 2). The snapshots during the cooling processes are shown in figure 8. Because of the inelastic collisions during the cooling process, the total energy of the system decreases. At the last stage of cooling, the velocity of particles becomes very small and the inhomogeneity of the system arises.

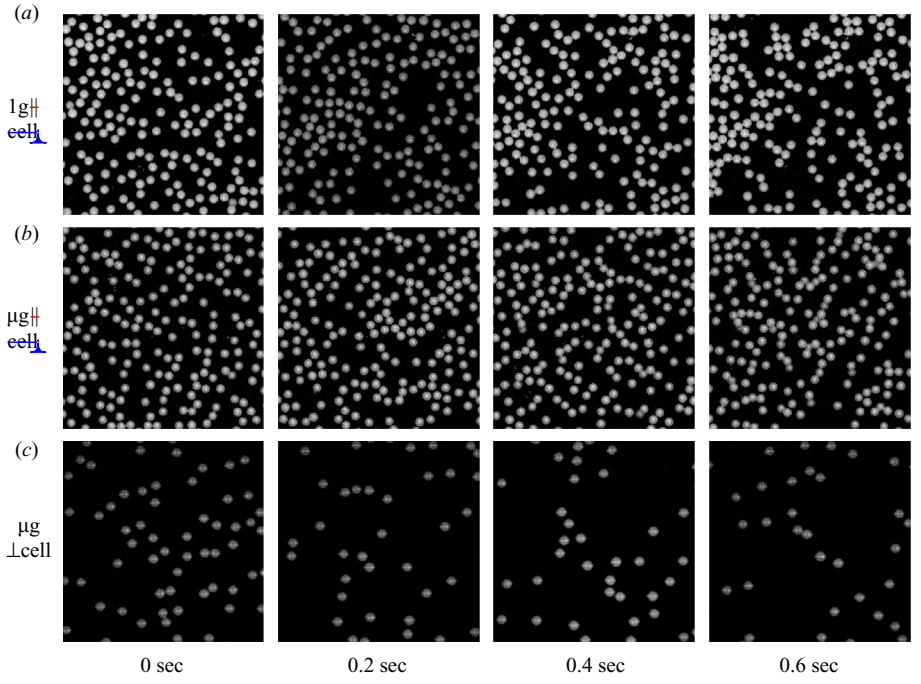

FIGURE 8. Snapshots during the cooling processes. (*a*) Horizontal cell under normal gravity condition. (*b*) Horizontal cell under microgravity condition. (*c*) Vertical cell under microgravity condition. The initial conditions are $f = 100\,\mathrm{Hz}$ and $A\omega^2 = 48\,\mathrm{m\,sec^{-2}}$ for the horizontal cell and $f = 40\,\mathrm{Hz}$ and $A\omega^2 = 250\,\mathrm{m\,sec^{-2}}$ for the vertical cell. The times shown at bottom indicate the elapsed time after the vibration is stopped.

The time evolution of T_g is shown in figure 9(*a*). The decay of T_g under microgravity condition and normal gravity condition is different in the form. Under microgravity condition, T_g decays with (1.1). From fitting, $\tau = 36 \pm 3\,\mathrm{msec}$ and $\gamma = 2.0 \pm 0.1$ are obtained for the horizontal cell, and $\tau = 38 \pm 4\,\mathrm{msec}$ and $\gamma = 2.1 \pm 0.1$ are obtained for the vertical cell. This algebraic decay sustains until 0.6–0.8 sec for both cells. On the contrary, under the normal gravity, it is hard to fit with (1.1). Based on the experimental results under microgravity condition, using the fitting values of τ, the rescaled temperature $T_g/T_0(1 + t/\tau)^2$ is plotted as a function of the elapsed time in figure 9(*b*), where the rescaled temperature under the normal gravity condition is clearly different from that of the microgravity condition. For microgravity condition, rescaled temperatures are almost 1 until 0.6–0.8 sec, which means that the decay of T_g obeys Haff's law with the restitution coefficient independent of the impact speed ($\gamma = 2$) (Haff 1983). In contrast, the decay of T_g for the normal gravity deviates from Haff's law soon after 0.2 sec.

5.2. *Velocity distribution function*

The VDF at the elapsed time t is obtained from the data set during $t \pm 25\,\mathrm{msec}$. For each VDF, the exponent β is obtained by fitting with (3.1). The VDFs at $t = 0$ (steady state), 100 and 300 msec for each condition are shown in figure 9(*c–e*). At $t = 0$, the exponent β is 1.55 for the horizontal cell under both the microgravity and normal gravity conditions, and β is 1.28 for the vertical cell under microgravity condition. The double-logarithmic plot of VDFs and time evolutions of β are shown in figure 10. In the horizontal cell under normal gravity condition, β is fluctuating around 1.5 for about 0.6 sec (figure 10*b*). Nonetheless, in the horizontal cell under microgravity

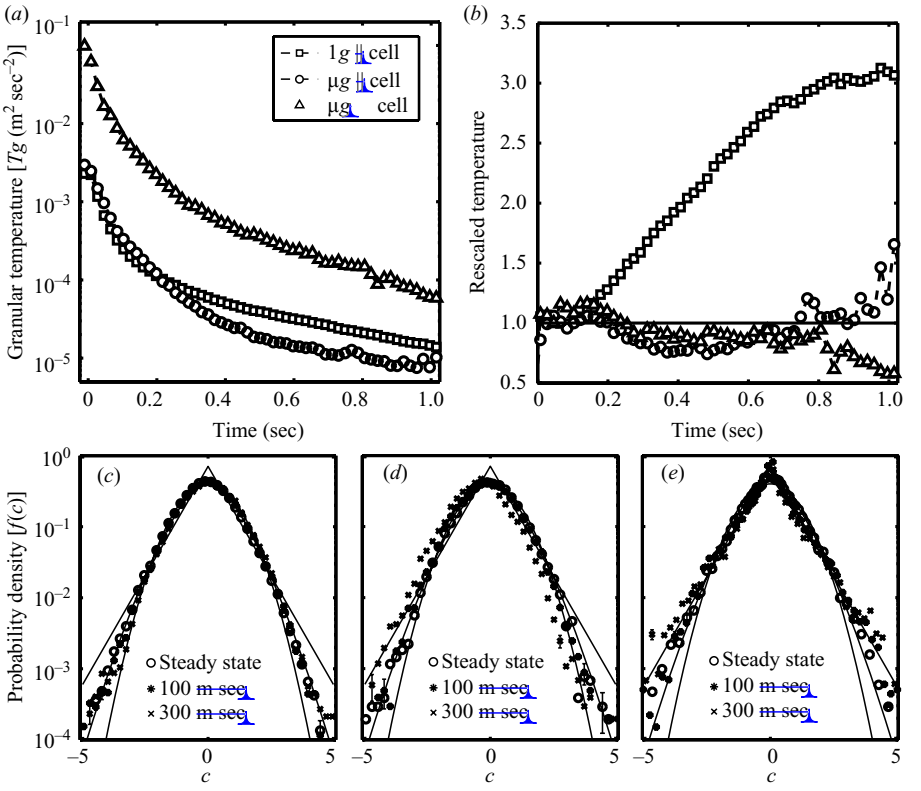

FIGURE 9. (*a*) Decay of T_g in the cooling state. (*b*) Time evolution of the rescaled temperature $T_g/T_0(1+t/\tau)^2$. The legends are common for plots in both (*a*) and (*b*). (*c–e*) VDF at $t=0$ (steady state), 100 and 300 msec for each condition. (*c*) Horizontal cell under the normal gravity. (*d*) Horizontal cell under microgravity condition. (*e*) Vertical cell under microgravity condition. The VDF in (*d*) shows an asymmetric shape for 300 msec. It is caused by the effect of g-jitter in the horizontal direction.

condition, β is fluctuating around 1.5 for $t<0.2$ sec, and decreases to 1 during $0.2\,\text{sec}<t<0.6\,\text{sec}$ (figure 10*d*). In the vertical cell under microgravity condition, β immediately decreases from 1.28 to 1 and is fluctuating around 1 (figure 10*f*).

In the cooling state, the theory by van Noije & Ernst (1998) predicts $\beta=1$ for the high energy tail. In our experiments under microgravity condition, the VDFs with $\beta=1$ are observed for both horizontal and vertical cells. However, under normal gravity condition, no agreement with the theory is found throughout the decaying process. In the horizontal cell under microgravity condition, β is almost 1.5 for the first 0.2 sec. In this setup, the particles with a large initial speed in the z-component can remain for a short time, which randomizes the system because of the glued beads on the top plate. The first 0.2 sec might be understood as the relaxation time for the randomization.

5.3. *The effect of g-jitter*

In the cooling state under the microgravity condition, the effect of g-jitter is estimated by R with $\delta g=0.01\,\text{m sec}^{-2}$, and τ^* is characterized by τ_{th} at each moment. Here R becomes 1 at $t=0.5$ and 1.0 sec for the horizontal and vertical cells, respectively. Thus, after these time periods, the effect of g-jitter cannot be neglected. The validity for $\delta g=0.01\,\text{m sec}^{-2}$ is shown in Appendix B.

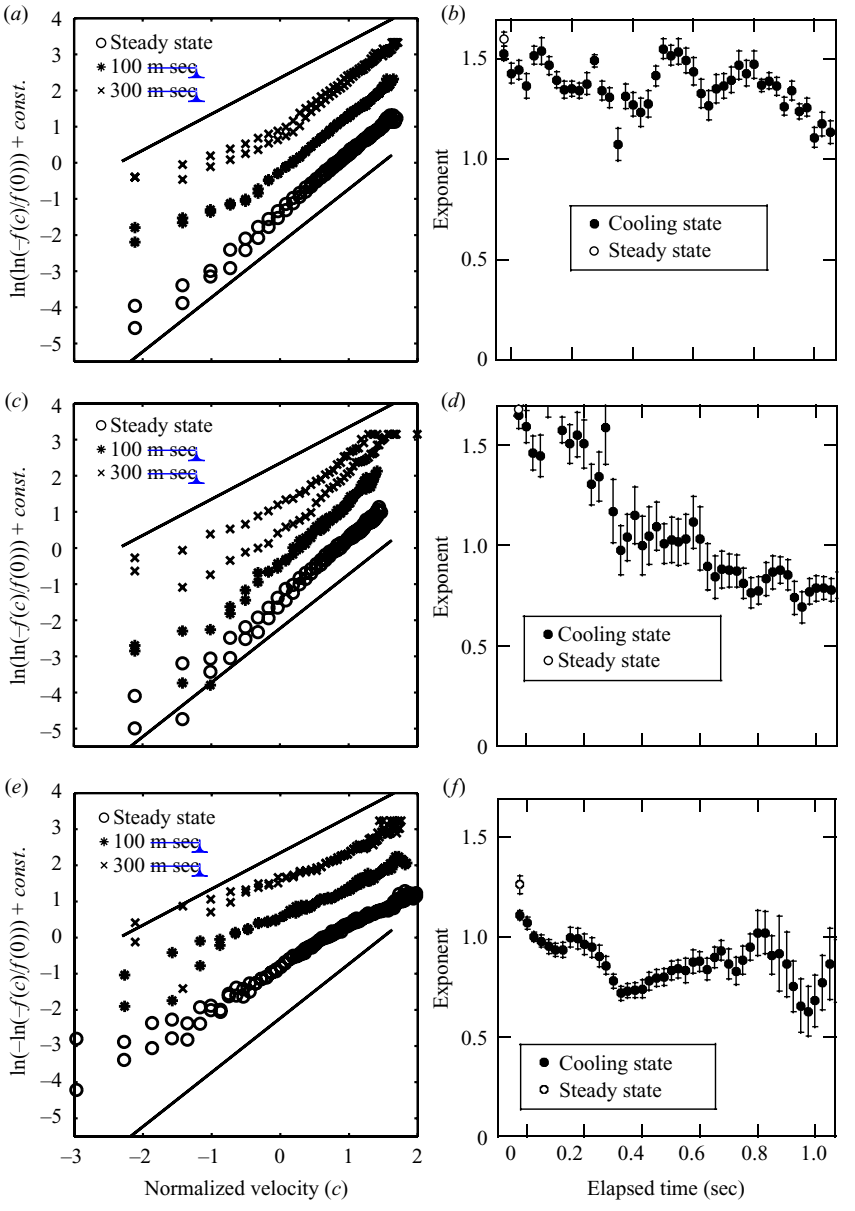

FIGURE 10. (a, c, e) Double-logarithmic plot of VDFs in the steady state (open circles), at $t = 100$ msec (asterisks) and 300 msec (crosses). The two solid lines guide the eyes for the slopes of 1 and 1.5. (b, d, f) Time evolution of the exponent β obtained by fitting. (a) and (b) Normal gravity condition in the horizontal cell. (c) and (d) Microgravity condition in the horizontal cell. (e) and (f) Microgravity condition in the vertical cell.

6. Discussion and conclusion

6.1. *Discussion*

We have conducted experiments on granular gas in detail, dominated by inelastic collisions in both the steady state and the cooling state. Present experiments under the microgravity condition allow us to reduce friction drastically.

The experiment for the steady state with sufficiently high acceleration produces similar results to those predicted by the theory of dilute granular gas with the white-noise thermostat (van Noije & Ernst 1998). Moreover, we found the scaling relation in the value D/T_g with respect to v_{pl}. When v_{pl} is large enough, D/T_g is almost independent of v_{pl} and the exponent of the VDF is close to 1.5 except for the case of low area fraction.

Strictly speaking, the theory that predicts VDF with the exponent of 3/2 is only applicable to high energy particles. Indeed, theory predicts that the shape of VDF at low energy is supposed to be Gaussian with a correction by the Sonine polynomials. Reis *et al.* (2007) fitted a deviation of VDF from Gaussian distribution by the one-dimensional Sonine polynomials well, and we also succeeded. However, we should note that the difference between the fitting by Sonine polynomials and fitting by the exponent of 3/2 is very small. A similar result has been reported in previous studies (Rouyer & Menon 2000). We still do not understand the reason why we observe the VDF with the exponent of 3/2 for the whole range of the velocity.

Theoretically, the relaxation time τ in (1.1) for the cooling process is predicted as $\tau^{-1} = 2\sqrt{\frac{T_0}{\pi}}(1-\varepsilon^2)\frac{1-(7/16)\phi}{(1-\phi)^2}\frac{\phi}{d}$ (Brilliantov & Pöschel 2004). Under microgravity condition, $T_0 = 27.4\,\mathrm{cm^2\,sec^{-2}}$ and $\phi = 0.313$ for the horizontal cell, and $T_0 = 1070\,\mathrm{cm^2\,sec^{-2}}$ and $\phi = 0.067$ for the vertical cell. Using $\varepsilon_{eff} = 0.62$, $\tau = 50$ and 60 msec are obtained for the horizontal and the vertical cells, respectively. These values are of the same order to the experimentally obtained values $\tau = 36 \pm 3$ msec and $\tau = 38 \pm 4$ msec for the horizontal and the vertical cells, respectively. We should note that, using $\varepsilon_{zir} = 0.95$, $\tau = 300$ and 400 msec are obtained for the horizontal and the vertical cells, respectively. These results suggest that the tangential friction between particles is not negligible, which is also found in numerical studies on the cooling state (Huthmann & Zippelius 1997; Luding *et al.* 1998).

6.2. *Conclusion*

In conclusion, under a condition of high enough acceleration, a universal form of the VDF with an exponent of 3/2 is observed for a wide range of velocities. Moreover, in this range, D/T_g which shows scaling relation on v_{pl} becomes constant.

The experiments in the vertical and the horizontal cells under microgravity condition provide an ideal system to study the freely cooling state of granular gas. Under the microgravity condition, the time evolution of the energy decay agrees with Haff's law (Haff 1983) by assuming a constant restitution coefficient. However, under the normal gravity condition, energy decay does not agree with Haff's law. The shape of the VDF satisfies an exponential distribution under microgravity condition which is consistent with the theory.

We thank Akinori Awazu, Igor Aranson, Harry Swinney and Danniel I. Goldman for their fruitful discussions; Y. Takahashi and K. Takeuchi for their help in microgravity experiments; and Ryo Suzuki for careful reading of the manuscript. This research is fully supported by the Japan Society for the Promotion of Science and the Japan Space Forum. The experiment involving parabolic flight was conducted with the help of the Diamond Air Service Co., for which we express our gratitude. S.T. thanks the Research Fellowships for Young Scientists from the Japan Society for the Promotion of Science 17-11808.

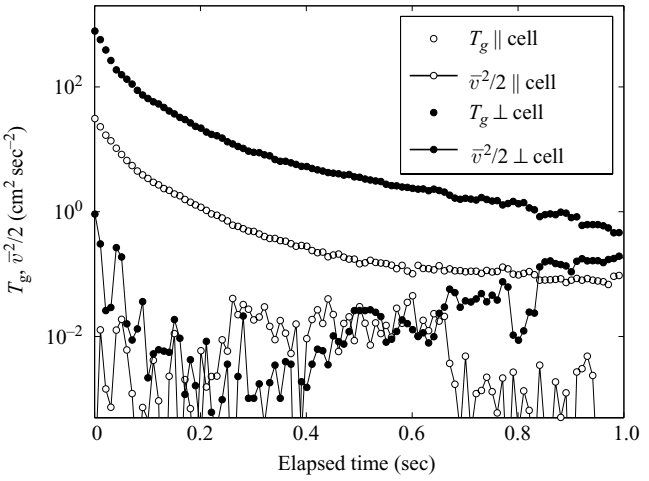

FIGURE 11. Time evolution of the T_g ~~(square)~~ and $\bar{v}^2$ ~~(circle)~~ is shown. Open ~~symbol~~ and solid ~~symbol~~ denote the results in the horizontal and vertical cells, respectively. Q2

Appendix A. Hydrodynamic interaction

Hydrodynamic loss between all the collision events is calculated theoretically from the packing fraction, the density of the particles, the diameter of the particles and the viscous coefficient of air as follows. First, we consider only the average loss of the systems. We can write the hydrodynamic interaction with air for each particle as

$$m\frac{\mathrm{d}v}{\mathrm{d}t} = -\mu v, \tag{A 1}$$

where m is the particle mass, v is the velocity of each particle and μ is the viscous coefficient by Stokes' law, $\mu = 3\pi d\eta$. Here d is the particle diameter, and η is the viscosity of air and is constant against air pressure. Note that this Stokes drag force is applicable in the small range of Reynolds number ($Re \leqslant 1$). In this case, Re is estimated as $Re = (UL)/(\eta/\rho_{air})$, where U and L are the typical velocity and the typical length of the system. Note that U and L, in our case, are the velocity and the diameter of each particle, and ρ_{air} is the density of air, which is 1.2×10^{-3} g cm^{-3} at 1 atm. Since the value of Re becomes $Re = U(\mathrm{cm\,sec^{-1}}) \times P(\mathrm{atm}) \times 6.7 \times 10^{-5}$, the typical velocity of this experiment is much less than the limitation value of Stokes' law. Then, the velocity decay due to viscosity is calculated as

$$\Delta v = -\frac{9\pi}{2\sqrt{2}}\frac{\eta}{\rho d}\frac{1-\phi}{\phi}, \tag{A 2}$$

where ϕ is the packing fraction and ρ is the net density of the particles. In our setup, the diameter of the particle is 1.0 mm, the net density is 6.0 g cm^{-3}, and the viscous coefficient η is 1.81×10^{-4} g cms^{-1}. Finally, we obtain a typical velocity decay between collisions at 6.6×10^{-2} mm sec^{-1} for the horizontal cell and 4.2×10^{-1} mm sec^{-1} for the vertical cell. As mentioned in the main text, these values are much smaller than the root mean square velocity of particles, and are therefore negligible.

Appendix B. Effect of g-jitter

We assess the effect of g-jitter in the cooling state quantitatively from the mean velocity of particles $\bar{v}$, where $\bar{v}$ is calculated for all the particles at each moment. Origin

of g-jitter in the parabolic flight mainly comes from manoeuvering of the aircraft and external wind. The frequency power spectrum of g-jitter fluctuations dominates at low frequency (<2 Hz). Since all the particles experience the same fluctuations of g-jitter, a final outcome of the effect should appear as a mean drift motion of particles, which can be detected by monitoring the mean velocity of particles. Figure 11 shows time evolutions of $\bar{v}^2$ and T_g for the horizontal cell and the vertical cell under microgravity. (Note that we subtracted the centre of mass velocity, $\bar{v}$, in calculating T_g throughout this paper.) When T_g is larger than $\bar{v}^2$, one can judge that the effect of g-jitter is negligible. As shown in figure 11, this condition holds until $t < 0.5$ sec for the horizontal cell, and until $t < 0.8$ sec for the vertical cell. These facts validate our estimation of $\delta g = 0.01\,\mathrm{m\,sec^{-2}}$ for cooling experiments given in § 5.

REFERENCES

Ahmad, S. R. & Puri, S. 2006 Velocity distributions in a freely evolving granular gas. *Euro. Phys. Lett.* **75** (1), 56–62.

Ahmad, S. R. & Puri, S. 2007 Velocity distributions and aging in a cooling granular gas. *Phys. Rev.* E **75**, 031302.

Aranson, I. S. & Olafsen, J. S. 2002 Velocity fluctuations in electrostatically driven granular media. *Phys. Rev.* E **66**, 061302.

Aspelmeier, T., Huthmann, M. & Zippelius, A. 2001 *Free Cooling of Particles with Rotational Degrees of Freedom*, Chapter 1, pp. 31–58. Lecture Notes in Physics, vol. 564. Springer.

Baxter, G. W. & Olafsen, J. S. 2003 Kinetics: gaussian statistics in granular gases. *Nature* **425**, 680.

Baxter, G. W. & Olafsen, J. S. 2007 Experimental evidence for molecular chaos in granular gases. *Phys. Rev. Lett.* **99**, 028001.

Blair, D. L. & Kudrolli, A. 2001 Velocity correlations in dense granular gases. *Phys. Rev.* E **64**, 050301(R).

Brilliantov, N. V., Poöschel, T., Kranz, W. T. & Zippelius, A. 2007 Translations and rotations are correlated in granular gases. *Phys. Rev. Lett.* **98**, 128001.

Brilliantov, N. V. & Pöschel, T. 2000 Velocity distribution in granular gases of viscoelastic particles. *Phys. Rev.* E **61** (5), 5573–5587.

Brilliantov, N. V. & Pöschel, T. 2004 *Kinetic Theory of Granular Gases*. Oxford University Press.

Das, S. K. & Puri, S. 2003 Kinetics of inhomogeneous cooling in granular fluids. *Phys. Rev.* E **68**, 011302.

Duran, J. 2000 *Sands, Powders, and Grains: An Introduction to the Physics of Granular Materials Series*. Springer.

Ernst, M. H., Trizac, E. & Barrat, A. 2006 The Boltzmann equation for driven systems of inelastic soft spheres. *J. Stat. Phys* **124** (2–4), 549–586.

Esipov, S. E. & Pöschel, T. 1997 The granular phase diagram. *J. Stat. Phys.* **86** (5/6), 1385–1395.

Falcon, E., Aumaître, S., Évesque, P., Palencia, F., Lecoutre-Chabot, C., Fauve, S., Beysens, D. & Garrabos, Y. 2006 Collision statistics in a dilute granular gas fluidized by vibrations in low gravity. *Europhys. Lett.* **74** (5), 830–836.

Fiscina, J. E. & Cáceres, M. O. 2007 Evaporation transition in vibro-fluidized granular matter. *Europhys. Lett.* **80**, 14007.

Géminard, J.-C. & Laroche, C. 2004 Pressure measurement in two-dimensional horizontal granular gases. *Phys. Rev.* E **70**, 021301.

Goldhirsch, I. 2003 Rapid granular flows. *Annu. Rev. Fluid Mech.* **35**, 267–293.

Goldhirsch, I., Noskowicz, S. H. & Bar-Lev, O. 2005 Nearly smooth granular gases. *Phys. Rev. Lett.* **95** (6), 068002.

Goldhirsch, I. & Zanneti, G. 1993 Clustering instability in dissipative gases. *Phys. Rev. Lett.* **70** (11), 1619–1622.

Goldshtein, A. & Shapiro, M. 1995 Mechanics of collisional motion of granular materials. Part 1. General hydrodynamics equations. *J. Fluid Mech.* **282**, 75–114.

Haff, P. K. 1983 Grain flow as a fluid-mechanical phenomenon. *J. Fluid Mech.* **134**, 401–430.

Hayakawa, H. & Kawarada, A. 2005 Granular gas in an experimental accessible setup. In *Powders and Grains*, vol. 2, pp. 1103–1106. Taylor & Francis. Q3

Herbst, O., Cafiero, R., Zippelius, A., Hermann, H. J. & Luding, S. 2005 A driven two-dimensional granular gas with coulomb friction. *Phys. Fluids* **17**, 107102.

Huthmann, M. & Zippelius, A. 1997 Dynamics of inelastically colliding rough spheres: relaxation of translational and rotational energy. *Phys. Rev.* E **56** (6), R6275.

Jaeger, H. M., Nagel, S. R. & Behringer, R. P. 1996 Granular solids, liquids, and gases. *Rev. Mod. Phys.* **68** (4), 1259–1273.

Jenkins, J. T. & Richman, M. W. 1985 Kinetic theory for plane flows of a dense gas of identical, rough, inelastic, circular disks. *Phys. Fluids* **28** (12), 3485.

Jenkins, J. T. & Zhang, C. 2002 Kinetic theory for identical, frictional, nearly elastic spheres. *Phys. Fluids* **14** (3), 1228.

Kawahara, R. & Nakanishi, H. 2004 Effects of velocity correlation on early stage of free cooling process of inelastic hard sphere system. *J. Phys. Soc. Japan* **73** (1), 68–75.

Kawarada, A. & Hayakawa, H. 2004 Non-Gaussian velocity distribution function in a vibrating granular bed. *J. Phys. Soc. Japan* **73** (8), 2037–2040.

Król, P. & Król, B. 2006 Determination of free surface energy values for ceramic materials and polyurethane surface-modifying aqueous emulsions. *J. Eur. Ceram. Soc.* **26** (12), 2241–2248.

Kudrolli, A., Wolpert, M. & Gollub, J. P. 1997 Cluster formation due to collisions in granular material. *Phys. Rev. Lett.* **78** (7), 1383–1386.

Labous, L., Rosato, A. D. & Dave, R. N. 1997 Measurements of collisional properties of spheres using high-speed video analysis. *Phys. Rev.* E **56** (5), 5717–5725.

Losert, W., Cooper, D. G. W., Delour, J., Kudrolli, A. & Gollub, J. P. 1999 Velocity statistics in excited granular media. *Chaos* **9** (3), 682–690.

Luding, S., Huthmann, M., McNamara, S. & Zippelius, A. 1998 Homogeneous cooling of rough, dissipative particles: theory and simulations. *Phys. Rev.* E **58** (3), 3416–3425.

Maass, C. C., Isert, N., Maret, G. & Aegerter, C. M. 2008 Experimental investigation of the freely cooling granular gas. *Phys. Rev. Lett.* **100**, 248001.

McNamara, S. & Young, W. R. 1994 Inelastic collapse in two dimensions. *Phys. Rev.* E **50** (1), R28–R31.

McNamara, S. & Young, W. R. 1996 Dynamics of a freely evolving, two-dimensional granular medium. *Phys. Rev.* E **53** (5), 5089–5100.

Miller, S. & Luding, S. 2004 Cluster growth in two- and three-dimensional granular gases. *Phys. Rev.* E **69**, 031305.

Mischeler, S. & Mouhot, C. 2006 Cooling process for inelastic Boltzmann equations for hard spheres. Part I. Self-similar solutions and tail behaviour. *J. Stat. Phys* **124** (2–4), 703–746.

Mischeler, S., Mouhot, C. & Richard, M. R. 2006 Cooling process for inelastic Boltzmann equations for hard spheres. Part I. The Cauchy problem. *J. Stat. Phys* **124** (2–4), 655–702.

Moon, S. J., Swift, J. B. & Swinney, H. L. 2004 Steady-state velocity distributions of an oscillated granular gas. *Phys. Rev.* E **69**, 011301.

Murayama, Y. & Sano, M. 1998 Transition from Gaussian to non-Gaussian velocity distribution functions in a vibrated granular bed. *J. Phys. Soc. Japan* **67** (6), 1826–1829.

Nie, X., Ben-Naim, E. & Chen, S. 2002 Dynamics of freely cooling granular gases. *Phys. Rev. Lett.* **89** (20), 204301.

Olafsen, J. S. & Urbach, J. S. 1998 Clustering, order, and collapse in a driven granular monolayer. *Phys. Rev. Lett.* **81** (20), 4369–4372.

Olafsen, J. S. & Urbach, J. S. 1999 Velocity distributions and density fluctuations in a granular gas. *Phys. Rev.* E **60** (3), R2468–R2471.

Painter, B., Dutt, M. & Behringer, R. P. 2003 Energy dissipation and clustering for a cooling granular material on a substrate. *Physica* D **175** (1), 43–68.

Pöschel, T., Brilliantov, N. V. & Formella, A. 2006 Impact of high-energy tails on granular gas properties. *Phys. Rev.* E **74**, 041302.

Reis, P. M., Ingale, R. A. & Shattuck, M. D. 2007 Forcing independent velocity distributions in an experimental granular fluid. *Phys. Rev.* E **75**, 051311.

Rouyer, F. & Menon, N. 2000 Velocity fluctuations in a homogeneous two-dimensional granular gas in steady state. *Phys. Rev. Lett.* **85** (17), 3676–3679.

Saitoh, K. & Hayakawa, H. 2007 Rheology of a granular gas under a plane shear. *Phys. Rev.* E **75** (2), 021302.

Santos, A. 2003 Transport coefficients of d-dimensional inelastic Maxwell models. *Physica* A **321** (3), 442.

Santos, A., Brey, J. J., Kim, C. S. & Dufty, J. W. 1989 Velocity distribution for a gas with steady heat flow. *Phys. Rev.* A **39** (1), 320–327.

Thornton, C. & Ning, Z. 1998 A theoretical model for the stick/bounce behaviour of adhesive, elastic–plastic spheres. *Powder Technol.* **99** (2), 154–162.

van Noije, T. P. C. & Ernst, M. H. 1998 Velocity distributions in homogeneous granular fluids: the free and the heated case. *Gran. Mat.* **1**, 57–64.

van Noije, T. P. C., Ernst, M. H. & Brito, R 1998 Ring kinetic theory for an idealized granular gas. *Physica* A **251** (1), 266–283.

van Zon, J. S., Kreft, J., Goldman, Daniel I., Miracle, D., Swift, J. B. & Swinney, Harry L. 2004 Crucial role of sidewalls in velocity distributions in quasi-two-dimensional granular gases. *Phys. Rev.* E **70**, 040301(R).

van Zon, J. S. & MacKintosh, F. C. 2005 Velocity distributions in dilute granular systems. *Phys. Rev.* E **72**, 051301.

Villani, C. 2006 Mathematics of granular materials. *J. Stat. Phys.* **124** (2–4), 781–822.

Wang, H.-Q. & Menon, N. 2008 Heating mechanism affects equipartition in a binary granular system. *Phys. Rev. Lett.* **100**, 158001.

Weir, G. & Tallon, S. 2005 The coefficient of restitution for normal incident, low velocity particle impacts. *Chem. Engng Sci.* **60** (13), 3637–3647.

Xu, H., Reeves, A. P. & Louge, M. Y. 2004 Measurement errors in the mean and fluctuation velocities of spherical grains from a computer analysis of digital images. *Rev. Sci. Instrum.* **75** (4), 811.